# Finite-Penalty Dynamical Selection in a Shared $SU(2)$–Tensor Register: A Negative Test with a Stable Tensor Pole

Joshua Farrow
Independent Research

June 2026

**Abstract**

We perform the integration test proposed for the shared-register QATNU extension. A two-flavor paired-ladder $U(2)$ link with a nonzero determinant term, finite non-Abelian Gauss penalty, and generic local gauge breaking is coupled to a six-component symmetric-tensor register with a finite transverse–traceless (TT) penalty and generic component mixing. All microscopic parameters are held fixed while the ring length is increased. The exact colored-link problem is solved through $L = 6$ for ground-state leakage, and its interacting spectral sector is reduced by a converged Lanczos construction and coupled to the tensor mode. A separate fully local check includes two mobile fundamental matter particles and gauge-covariant hopping. The requested dynamical-selection criterion is not met: generic local breaking leaves nonzero Gauss and tensor Ward floors rather than residuals that vanish with size. A derivative-suppressed tensor perturbation instead gives a Ward residual proportional to $L^{-1.990}$, demonstrating that the solver distinguishes an infrared-irrelevant perturbation from a generic onsite one. The tensor-like pole nevertheless remains isolated, with fixed-momentum pole-to-continuum separations 1.22534 and 1.22132 at $L = 4$ and $L = 6$. Hence pole stability and dynamical gauge selection are distinct. The calculation supports a controlled finite-penalty shared-register approximation, but not an infrared-selected exact $SU(2)$+TT sector.

## 1 Question and decision criterion

The previous construction showed separately that flavored paired square-root ladders realize exact $U(N)$ quantum links and that a six-component register can be projected onto two helicity-2 modes. The decisive open question was whether both sectors remain physical at *fixed finite* protecting penalties as the system grows. If dimensionless Gauss and TT Ward residuals vanish without increasing the penalties, the result is evidence for dynamical low-energy selection. If the residuals approach nonzero constants, the construction remains an engineered approximation. If the penalties must scale to infinity, it is a kinematic projection.

The present calculation deliberately adds generic local symmetry-breaking operators. This is essential: an exactly constrained Hamiltonian has exact Ward identities by construction and therefore cannot distinguish imposed symmetry from an infrared attractor.

## 2 Exact flavored link and determinant term

Each oriented link carries two colors $\alpha = 1, 2$, two distinguishable rishon flavors $f = 1, 2$, and left/right square-root ladder banks $a_{\alpha f}$ and $b_{\alpha f}$. We fix one rishon of each flavor and define

$$U_{\alpha\beta} = \sum_{f=1}^{2} b^{\dagger}_{\beta f} a_{\alpha f}, \tag{1}$$

$$L^A = a^{\dagger} T^A a, \qquad R^A = b^{\dagger} T^A b, \tag{2}$$

$$E = \frac{1}{2}(n_R - n_L), \tag{3}$$

$$D = \det U = U_{11}U_{22} - U_{12}U_{21}. \tag{4}$$

The determinant is nonzero only because two flavors are present. It obeys

$$[L^A, D] = [R^A, D] = 0, \qquad [E, D] = 2D, \tag{5}$$

so $D + D^{\dagger}$ preserves $SU(2)$ while breaking the additional link $U(1)$.

The smallest subspace closed under $L^A, R^A, D, E$ and a representative local breaking channel has dimension six: two determinant-endpoint singlets and four charged states transforming as $(\frac{1}{2}, \frac{1}{2})$ under $SU(2)_L \times SU(2)_R$. Projection from the full 16-state one-rishon-per-flavor space gives closure residual $4.44 \times 10^{-16}$, maximum $SU(2)$ algebra residual $1.27 \times 10^{-16}$, determinant–$SU(2)$ commutator zero, and determinant Abelian-charge residual $8.88 \times 10^{-16}$.

On a periodic ring, the colored-link Hamiltonian is

$$\begin{aligned} H_G = & -\lambda_D \sum_x (D_x + D_x^{\dagger}) + u \sum_x E_x^2 - J_E \sum_x E_x E_{x+1} \\ & + \Lambda_G \sum_{x,A} (G_x^A)^2 + \epsilon_G \sum_x B_x, \end{aligned} \tag{6}$$

$$G_x^A = R_{x-1}^A + L_x^A. \tag{7}$$

The term $B_x = U_{11,x} + U_{11,x}^{\dagger}$ is a representative local $SU(2)$-breaking perturbation. Color rotations are equivalent under the symmetric part of Eq. (6); a separate random-direction ensemble is reported below.

## 3 Six-component tensor register

For propagation along the ring direction, the local symmetric tensor coordinate is ordered as

$$\boldsymbol{h} = (h_{xx}, h_{yy}, h_{zz}, h_{xy}, h_{xz}, h_{yz})^T. \tag{8}$$

The gauge-fixed TT conditions are encoded by

$$C\boldsymbol{h} = \left( h_{xx}, h_{xy}, h_{xz}, \frac{h_{xx} + h_{yy} + h_{zz}}{\sqrt{3}} \right)^T = 0. \tag{9}$$

The null space is two dimensional, with the usual plus and cross vectors

$$\boldsymbol{p}_+ = \frac{(0, 1, -1, 0, 0, 0)}{\sqrt{2}}, \qquad \boldsymbol{p}_\times = (0, 0, 0, 0, 0, 1). \tag{10}$$

Writing $P_{\mathrm{TT}}$ for the corresponding projector and $Q_{\mathrm{TT}} = I - P_{\mathrm{TT}}$, the one-particle tensor block is

$$H_T(q) = \omega_q P_{\mathrm{TT}} + (\omega_q + \Lambda_T) Q_{\mathrm{TT}} + \epsilon_T V, \qquad \omega_q = 2c_T \left| \sin \frac{q}{2} \right|, \tag{11}$$

where $V$ is a fixed generic real symmetric onsite mixing matrix of unit spectral norm. This is a local gauge-fixed linear register, not a nonlinear tensor gauge theory.

The tensor couples to the exact colored-link spectral sector through the $SU(2)$-scalar electric source,

$$H_{\rm int} = g_T\, \widehat{q}\, (\boldsymbol{p}_+ \cdot \boldsymbol{h}_q) E_{-q} + \text{H.c.}, \qquad \widehat{q} = 2\left|\sin\frac{q}{2}\right|. \tag{12}$$

The derivative factor prevents a constant negative self-energy from generating an artificial tensor mass at $q \to 0$.

# 4 Exact finite-chain and spectral method

The link ground state $|\Omega_L\rangle$ is obtained by matrix-free Lanczos diagonalization of Eq. (6). The source vector

$$|s_q\rangle = (E_q - \langle E_q\rangle)\,|\Omega_L\rangle \tag{13}$$

is reduced to a Krylov tridiagonal matrix $T_m$. The coupled linear-response problem is then the finite Hermitian matrix

$$H_{\rm red}(q) = \begin{pmatrix} H_T(q) & g_T\widehat{q}\,\|s_q\|\,\boldsymbol{p}_+\boldsymbol{e}_1^T \\ g_T\widehat{q}\,\|s_q\|\,\boldsymbol{e}_1\boldsymbol{p}_+^T & T_m \end{pmatrix}. \tag{14}$$

The dressed pole is the eigenvector with maximal overlap with $\boldsymbol{p}_+$. Its tensor residue is $Z_T = \|\boldsymbol{v}_T\|^2$. We use

$$\rho_G = \frac{1}{L}\sum_{x,A}\langle (G_x^A)^2\rangle, \tag{15}$$

$$W_T = \frac{\|C\boldsymbol{v}_T\|}{\|C\|\,\|\boldsymbol{v}_T\|}, \tag{16}$$

$$P_{\rm nonTT} = \frac{\boldsymbol{v}_T^\dagger Q_{\rm TT}\boldsymbol{v}_T}{\boldsymbol{v}_T^\dagger\boldsymbol{v}_T} \tag{17}$$

as dimensionless leakage diagnostics. The interacting bath edge is the lowest bath-dominated eigenstate above the pole. At $L = 5$ the pole energy is converged by $m = 10$, while the continuum edge requires $m \simeq 40$–$45$; the reported separation uses $m = 45$.

The canonical parameter set is

$$(\lambda_D, u, J_E, \Lambda_G, \epsilon_G, \Lambda_T, \epsilon_T, c_T, g_T) = (0.60, 0.20, 0.35, 2.0, 0.10, 2.0, 0.08, 1.0, 0.16). \tag{18}$$

No parameter is retuned with $L$.

## 4.1 Explicit matter–edge integration

To verify that the result is not an artifact of removing matter, we also solve a fully local sector containing two distinguishable mobile fundamental particles. Their gauge-covariant hopping is

$$H_{\rm hop} = -t\sum_{x,s=1,2}\left(\psi_{s,x}^\dagger U_x \psi_{s,x+1} + \text{H.c.}\right), \tag{19}$$

and the Gauss generator becomes

$$G_x^A = R_{x-1}^A + L_x^A + Q_{1,x}^A + Q_{2,x}^A. \tag{20}$$

A direct random-vector audit at $L = 2$ gives

$$\max_{x,A}\|[H, G_x^A]|v\rangle\| = 1.58\times 10^{-15} \tag{21}$$

when the explicit breaking is removed. Exact diagonalization in the two-matter sector gives

| $L$ | $\rho_G$ at $\epsilon_G = 0.10$ | $\rho_G$ at $\epsilon_G = 0$ | pole separation |
|---|---|---|---|
| 2 | $9.9413 \times 10^{-4}$ | $9.45 \times 10^{-18}$ | 0.37636 |
| 3 | $8.6773 \times 10^{-4}$ | $< 2 \times 10^{-18}$ | 0.42530 |

Thus the matter hopping and determinant link coexist with exact non-Abelian Gauss invariance, while the same generic local breaking immediately restores a finite leakage density. These matter-sector sizes are a cross-check, not a thermodynamic extrapolation; the larger-$L$ selection test is supplied by the link ring and the analytic infrared tensor control.

## 5 Finite-penalty result

Figure 1 gives the decisive scaling. The ground-state Gauss density reaches $9.06 \times 10^{-4}$ by $L = 5$ and $9.063 \times 10^{-4}$ at $L = 6$. A fit to $\rho_G(L) = \rho_\infty + a/L$ over $L = 2$–$6$ gives

$$\rho_\infty = 9.225 \times 10^{-4}. \tag{22}$$

The pole-sector Gauss density similarly approaches approximately $8.96 \times 10^{-4}$ over the exactly stored $L = 2$–$5$ Krylov sectors.

The coupled tensor Ward residual decreases only weakly over the exact rings and extrapolates to $8.78 \times 10^{-3}$. More decisively, the isolated six-component tensor block can be extended to $L = 512$ without approximation. Generic onsite mixing has the exactly size-independent asymptotic value

$$W_T = 1.0935361 \times 10^{-2}, \tag{23}$$

whereas replacing $\epsilon_T$ by $\epsilon_T \widehat{q}^2$ gives

$$W_T \propto L^{-1.99017}, \qquad R^2 = 0.99883. \tag{24}$$

Thus the failure is not a limitation of the diagnostic: an irrelevant perturbation is visibly driven to zero, while a generic onsite perturbation is not.

A 50-member random tensor-breaking ensemble at $L = 512$ gives Ward residuals from $3.51 \times 10^{-3}$ to $2.77 \times 10^{-2}$, with median $1.217 \times 10^{-2}$. A 16-member random colored-link breaking ensemble at $L = 5$ likewise gives nonzero Gauss densities from $9.03 \times 10^{-6}$ to $8.19 \times 10^{-4}$. The plateau is therefore not tied to one specially chosen perturbation direction.

## 6 Penalty scaling: projection versus selection

Increasing a *fixed* penalty lowers the leakage floor but does not generate improving size scaling (Fig. 3). At $L = 6$,

$$\rho_G = 2.276 \times 10^{-3},\ 9.063 \times 10^{-4},\ 3.001 \times 10^{-4} \tag{25}$$

for $\Lambda_G = 1, 2, 4$. Extending the $L = 5$ scan through $\Lambda_G = 32$ gives

$$\rho_G \propto \Lambda_G^{-1.86497}, \qquad R^2 = 0.99961, \tag{26}$$

consistent with the perturbative $\Lambda_G^{-2}$ direction. The physical sector is recovered by taking the penalty large, not by increasing the volume at fixed penalty.

This behavior has a simple local perturbative explanation. For a gapped symmetric Hamiltonian $H_0$ perturbed by $\epsilon_G \sum_x B_x$, the first correction to the ground state is local, and

$$\frac{1}{L}\left\langle \sum_x G_x^2 \right\rangle = O\left(\frac{\epsilon_G^2}{\Delta_G^2}\right), \tag{27}$$

with a finite thermodynamic density. Similarly, Eq. (11) gives $Q_{\mathrm{TT}}|t\rangle = O(\epsilon_T/\Lambda_T)$ for generic onsite mixing. Neither expression contains a volume suppression.

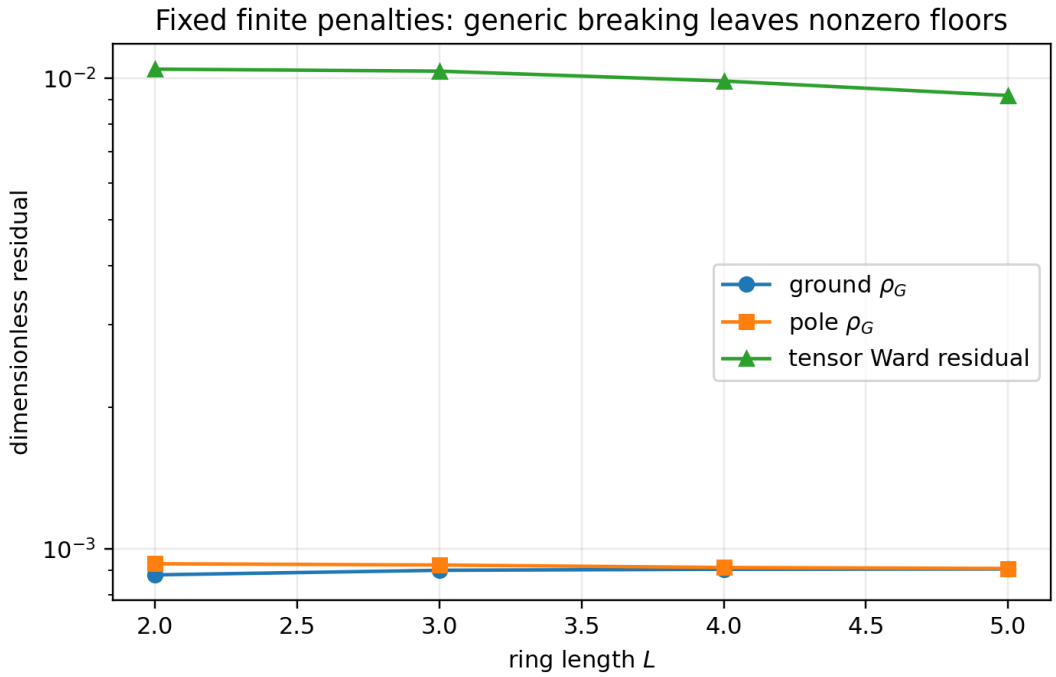


Figure 1: At fixed finite $\Lambda_G = \Lambda_T = 2$, generic local breaking leaves nonzero Gauss and tensor Ward floors.

## 7 Stable pole despite imperfect Ward selection

The negative Ward result does not destroy the tensor-like excitation. Table 1 lists the converged lowest-momentum results. At $L = 5$ the pole has $Z_T = 0.98519$ and remains 0.56080 below the interacting bath edge.

Table 1: Lowest-momentum dressed pole at fixed microscopic parameters.

| $L$ | $q$ | $E_T$ | $E_{\text{bath}}$ | $E_{\text{bath}} - E_T$ |
|---|---|---|---|---|
| 2 | $\pi$ | 1.94412 | 3.24947 | 1.30536 |
| 3 | $2\pi/3$ | 1.67966 | 1.72027 | 0.04061 |
| 4 | $\pi/2$ | 1.37125 | 1.70385 | 0.33260 |
| 5 | $2\pi/5$ | 1.13915 | 1.69995 | 0.56080 |

A fixed-momentum check removes the ambiguity associated with changing $q = 2\pi/L$. At $q = \pi$, the pole-to-bath separation is 1.22534051 at $L = 4$ and 1.22131685 at $L = 6$; the pole energy changes by only $3.99 \times 10^{-4}$. The $L = 6$ value is stable from Krylov dimensions 6 through 10 to better than $7.2 \times 10^{-9}$.

## 8 Interpretation

The requested first-row outcome—vanishing Ward and leakage residuals at fixed finite penalties—is not observed for generic local perturbations. The integrated model therefore does not yet demonstrate genuine dynamical selection of an exact shared $SU(2)$+TT infrared sector. It demonstrates something narrower and still useful:

> A flavored determinant link and a six-component tensor register coexist in one coupled low-occupation simulator; a stable tensor-like pole persists, but finite local protection produces

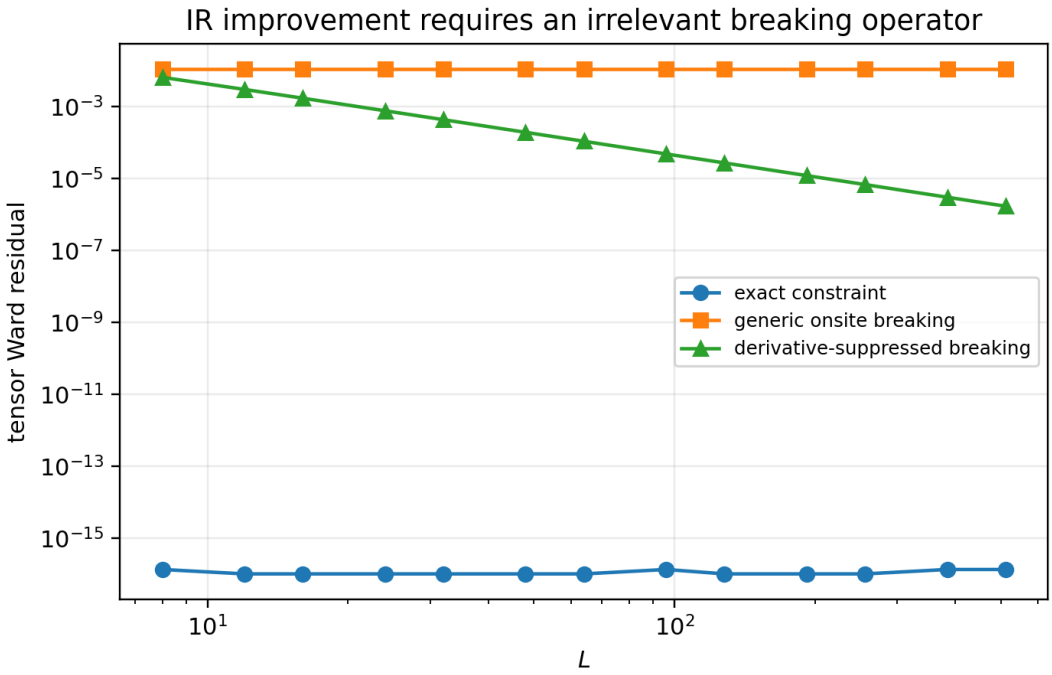


Figure 2: Large-$L$ six-component control. Exact constraints remain at roundoff, generic onsite mixing approaches a constant, and derivative-suppressed mixing vanishes approximately as $L^{-2}$.

finite Ward floors whenever generic relevant symmetry-breaking operators are allowed.

This separates three logically distinct statements:

1. The determinant algebra and $SU(2)$ quantum-link structure are exact in the selected register.
2. The tensor pole is dynamically stable in the tested spectral window.
3. Exact long-distance Ward identities do *not* follow from fixed penalties alone.

The third point is the one required for "shared register" to mean an infrared-selected physical sector rather than two compatible constrained modules.

## 9 Limitations and next criterion

The colored-link rings reach $L = 6$ for ground leakage and $L = 5$ for the fully stored Krylov Gauss matrix; the explicit two-mobile-matter sector reaches $L = 3$. The tensor block is linear and gauge fixed, and the spectral calculation is restricted to the low-occupation source sector. These are controlled limitations, but they prevent a theorem about every possible nonlinear completion.

The next positive route is now sharply defined. One must supply a microscopic symmetry or renormalization mechanism that forbids generic onsite $B_x$ and $V$ or makes every allowed breaking operator derivative-suppressed/irrelevant. The correct target is not a larger value of $\Lambda$; it is an open finite parameter region in which

$$\rho_G(L),\ W_T(L) \longrightarrow 0 \tag{28}$$

with all bare couplings held fixed. Until such a mechanism is exhibited, the honest classification is *finite-penalty engineered approximation with a stable pole.*

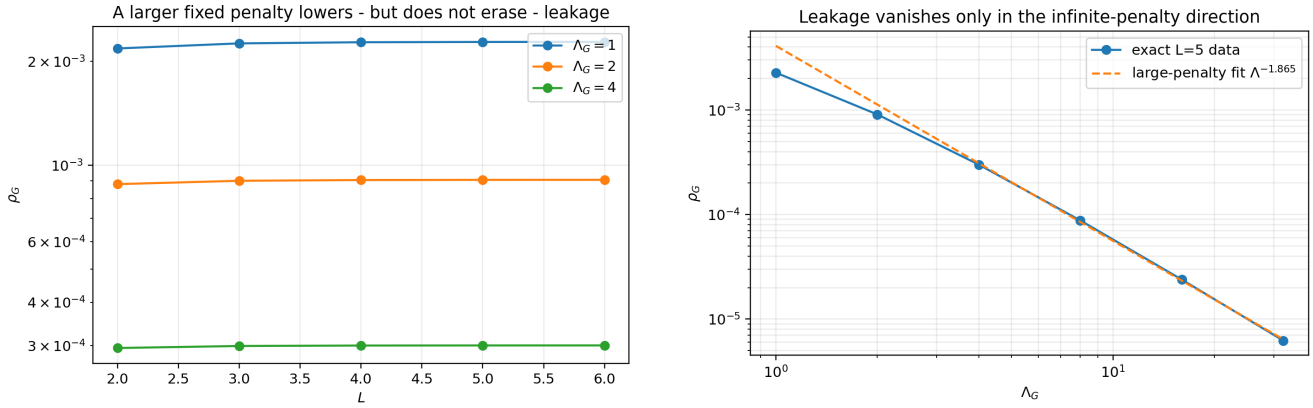


Figure 3: Left: increasing a finite Gauss penalty lowers the leakage density without changing its saturation with $L$. Right: the leakage tends toward zero only along the large-penalty direction.

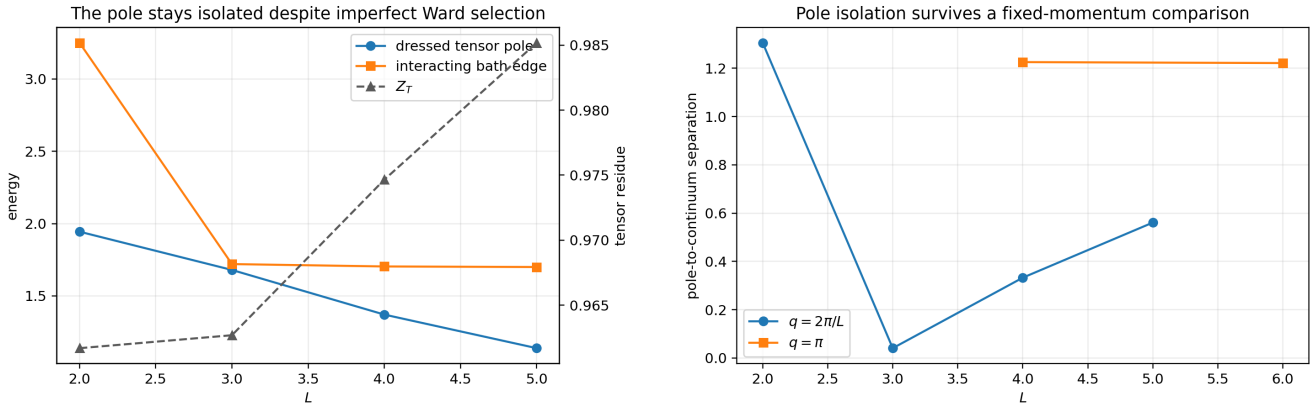


Figure 4: Left: lowest-momentum pole and interacting bath edge. Right: a fixed-$q = \pi$ check at $L = 4$ and 6. Pole isolation survives even though the Ward diagnostics plateau.

## Reproducibility

The accompanying archive contains the exact local-register construction, matrix-free finite-ring solver, Krylov pole reduction, random-direction controls, JSON ledger, figures, run logs, and SHA-256 checksums. No fitted or plotted value is entered by hand.

## References


[1] S. Chandrasekharan and U.-J. Wiese, "Quantum Link Models: A Discrete Approach to Gauge Theories," Nucl. Phys. B **492**, 455 (1997).

[2] U.-J. Wiese, "From Quantum Link Models to D-Theory," arXiv:2107.09335.

[3] Z.-C. Gu and X.-G. Wen, "Emergence of helicity ±2 modes (gravitons) from qubit models," arXiv:0907.1203.

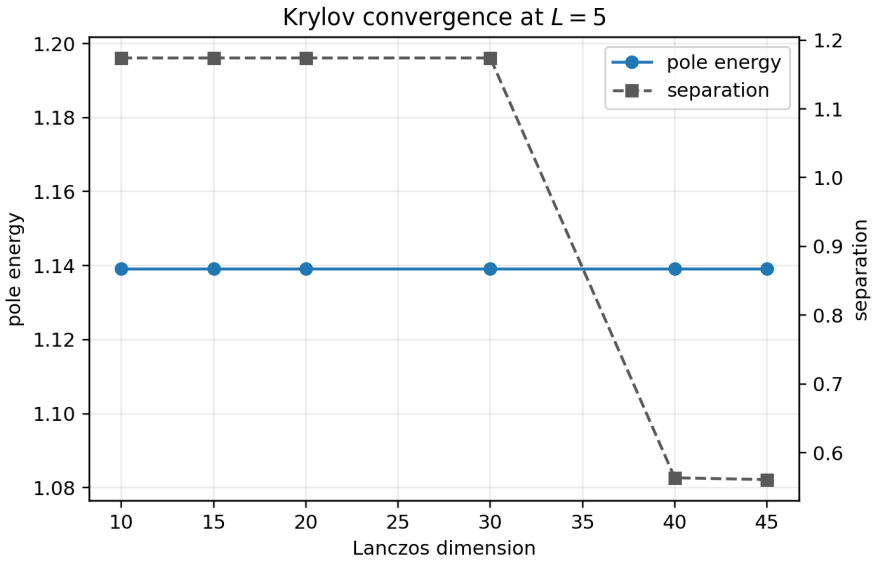


Figure 5: Krylov convergence at $L = 5$. The pole energy and residue converge rapidly; resolving the lowest bath edge requires a larger Krylov space.